Electromagnetic instabilities for relativistic beam-plasma interaction in whole *k* space: Nonrelativistic beam and plasma temperature effects

A. Bret*
ETSI Industriales, Universidad de Castilla–La Mancha, 13071 Ciudad Real, Spain

M.-C. Firpo†
Laboratoire de Physique et de Technologie des Plasmas (CNRS-UMR 7648), Ecole Polytechnique, 91128 Palaiseau Cedex, France

C. Deutsch‡
Laboratoire de Physique des Gaz et des Plasmas (CNRS-UMR 8578), Université Paris XI, Bâtiment 210, 91405 Orsay Cedex, France
(Received 2 July 2004; revised manuscript received 11 April 2005; published 19 July 2005)

For the system formed by a relativistic electron beam and its plasma return current, we investigate the effects of both transverse and parallel beam and plasma temperatures on the linear stability of collective electromagnetic modes. We focus on nonrelativistic temperatures and wave-vector orientations ranging from two-stream to filamentation instabilities. Water-bag distributions are used to model temperature effects and we discuss their relevance. Labeling θ_k the angle between the beam and the wave vector, one or two critical angles $\theta_{c,i}$ are determined exactly and separate the **k** space into two parts. Modes with $\theta_k<\theta_c=\min(\theta_{c,i})$ are quasilongitudinal and poorly affected by any kind of temperature. Modes having $\theta_k>\theta_c$ are very sensitive to transverse beam and plasma parallel temperatures. Also, parallel plasma temperature can trigger a transition between the beam-dependent filamentation instability ($\theta_k=\pi/2$) and the plasma-temperature-dependent Weibel instability so that two-stream, filamentation, and Weibel instabilities are eventually closely connected to each other. The maximum growth rate being reached for a mode with $\theta_k<\theta_c$, no temperature of any kind can significantly reduce it in the nonrelativistic temperature regime.

DOI: 10.1103/PhysRevE.72.016403 PACS number(s): 52.35.Qz, 52.35.Hr, 52.50.Gj, 52.57.Kk

I. INTRODUCTION

The fast ignition scenario (FIS) concept [1], where an ultrashort laser impulsion is used to ignite a precompressed target, implies the interaction of a relativistic electron beam (REB) generated by the laser impulsion with a hot and dense plasma. The REB passing through the plasma quickly creates a return current, and the resulting (magnetically neutralized) system is known to undergo various linear electromagnetic instabilities, namely the two-stream, filamentation, and Weibel instabilities. For clarity, it is convenient to classify them in terms of their wave-vector orientation **k** with respect to their electric field eigenmodes $\mathbf{E_k}$ and to the beam velocity $\mathbf{V}_b$. Their origin is also relevant. The two-stream instability has its wave vector aligned with both the beam and the electric field ($\mathbf{k}\|\mathbf{V}_b,\mathbf{k}\|\mathbf{E_k}$). The filamentation instability has its wave vector normal to the beam and to its electric field ($\mathbf{k}\perp\mathbf{V}_b,\mathbf{k}\perp\mathbf{E_k}$). These two instabilities are "beam based," which means they need a beam to exist. On the other hand, the Weibel instability [2] is "temperature anisotropy based," which means it can develop from a temperature anisotropy in the plasma even without any beam. Weibel modes are purely transverse and their wave vector is normal to the high-temperature axis. This corresponds rigorously to the original configuration studied by Weibel [2], although it is also commonplace (see Refs. [3,4] for example) to generically label as Weibel modes what we just labeled as "filamentation" [5]. In the present work, we rather choose (as in Ref. [6]) to be consistent with the original Weibel setting and to refer to the unstable transverse modes with wave vector normal to the beam as "filamentation instability."

A large amount of work [3,7–16] has recently been devoted to those stability issues motivated by the FIS scenario, and some authors [3,9] have pointed out the need to analyze the coupling between two-stream and filamentation instabilities. What do we exactly intend by coupling in this linear setting? It has to do with the orientation of the wave vector. Indeed, two-stream and filamentation instabilities correspond to extreme orientation of the wave vector. Since the real world is found back summing over the whole **k** space, it is important to investigate instabilities with every possible orientations of **k** ranging from the two-stream orientation to the filamentation one.

In a recent publication [17], we systematically investigated the electromagnetic instabilities in the whole **k** space for a cold relativistic beam interacting with a transversely hot plasma, using the most general electromagnetic formalism. The electrostatic, or longitudinal, approximation would only capture longitudinal modes and therefore would fail to recover both Weibel and filamentation instabilities. As a matter of fact, it has long been known that two-stream and filamentation instabilities pertain to the same two-stream/filamentation (TSF) branch [18] so that the angle $(\widehat{\mathbf{k},\mathbf{E_k}})$ evolves from 0 to $\pi/2$ along this branch. The investigation of this branch unravels two major **k**-oblique effects: (i) There is a critical angle θ_c for which waves are unstable at any k; (ii) as soon as the beam is relativistic, the absolute maximum

*Electronic address: antoineclaude.bret@uclm.es
†Electronic address: firpo@lptp.polytechnique.fr
‡Electronic address: claude.deutsch@pgp.u-psud.fr

growth rate is reached for a wave vector making an oblique angle with the beam. These results show the minimum requirements to obtain the two "oblique effects" mentioned just above: one normal plasma temperature and a relativistic beam. Plasma (or beam [5]) normal temperature prompts a critical angle in the **k** space while the all **k** maximum growth rate on the TSF branch departs from the beam axis as soon as it is relativistic (see also [19]).

Starting, therefore, from this configuration, our aim in this paper is to investigate the effects of every possible other temperature, namely plasma parallel temperature plus beam parallel and transverse temperature. We shall "add" one temperature at a time in order to clearly identify its effects before turning to the more general case. Two-stream and filamentation instabilities will be detailed each time we add a temperature.

The electromagnetic formalism also recovers the Weibel modes. These modes can turn unstable in the presence of some strong temperature anisotropy of the plasma, whether there is a beam or not. They may appear on another branch than the one bearing the two-stream and filamentation instabilities [17] (although they can also be seen on the TSF branch with the proper anisotropy in the plasma; see Sec. V for details). We shall not study this last branch here and shall restrict ourselves to the TSF one. The maximum growth rate of the Weibel modes all over the **k** space is usually smaller than the maximum TSF one, even for an infinite anisotropy of temperature [17]. Furthermore, we consider here a fusion plasma where the electronic distribution before the beam hits it should rather be isotropic, that is, Weibel stable.

The article is structured as follows. The theoretical framework is introduced in Sec. II, together with the basic model displaying the main oblique effects. We start analyzing transverse beam temperature effects in Sec. III before we turn to parallel beam temperature influence in Sec. IV. We then investigate parallel plasma temperature effects in Sec. V and consider the general case in Sec. VI before we reach our conclusions. The reader interested in the final result can jump directly to Sec. VI where all temperatures are accounted for together. Simply put, we consider here a hot relativistic electron beam interacting with a hot plasma. Temperatures are taken nonrelativistic (which still allows us to explore temperatures up to tens of keV). The main result of this paper is that the highest growth rate of the TSF branch is located away from the main wave-vector axis regardless of any parallel or transverse plasma or beam temperature. Furthermore, this growth rate is almost insensitive to temperatures.

II. THEORETICAL FRAMEWORK

We consider a homogeneous, spatially infinite, collisionless, and unmagnetized plasma whose dynamics is ruled by the relativistic Vlasov-Maxwell equations for the electronic distribution function $f(\mathbf{p},\mathbf{r},t)$ and the electromagnetic field. Ions are assumed to form a fixed neutralizing background. Within the linear approximation, the dielectric tensor elements are [20,21]

$$\varepsilon_{\alpha\beta} = \delta_{\alpha\beta} + \frac{\omega_{\mathrm{pe}}^2}{n_e\omega^2}\int \frac{p_\alpha}{\gamma}\frac{\partial f_0}{\partial p_\beta}d^3p + \frac{\omega_{\mathrm{pe}}^2}{n_e\omega^2}\int \frac{p_\alpha p_\beta}{\gamma}\frac{\mathbf{k}\cdot\partial f_0/\partial \mathbf{p}}{m_e\gamma\omega - \mathbf{k}\cdot\mathbf{p}}d^3p, \quad (1)$$

where the integrals must be evaluated using the standard Landau contour for a proper kinetic treatment. The plasma frequency is given by $\omega_{\mathrm{pe}}=\sqrt{4\pi n_e q^2/m_e}$, with n_e the electron density and m_e the electron mass. The relativistic factor $\gamma=\sqrt{1+p^2/(m_e^2c^2)}$ couples the integration along the three dimensions of the momentum space.

The beam velocity is aligned with the z axis and the wave vector lies in the (x,z) plan. We define $\theta_{\mathbf{k}}=(\widehat{\mathbf{e}_z,\mathbf{k}})$ so that the two-stream configuration corresponds to $\theta_{\mathbf{k}}=0$ and filamentation to $\theta_{\mathbf{k}}=\pi/2$. Here the distribution function f_0 we are starting with consists in the sum of a beam term f_0^b and a plasma term f_0^p with

$$f_0^p = \frac{n_p}{(2P_{tp\perp})^2}[\Theta(p_x+P_{tp\perp})-\Theta(p_x-P_{tp\perp})][\Theta(p_y+P_{tp\perp}) - \Theta(p_y-P_{tp\perp})]\delta(p_z+P_p), \quad (2)$$

and

$$f_0^b = n_b\delta(p_x)\delta(p_y)\delta(p_z-P_b). \quad (3)$$

We set $P_{b,p}=m_e\gamma_{b,p}V_{b,p}$, with $V_{b,p}$ beam and plasma drift velocities. Additionally, $n_pV_p=n_bV_b$ reflects current neutralization with $n_{b,p}$ beam and plasma electron densities. $\Theta(x)$ denotes the Heaviside step function. Such waterbag distributions provide a classical tool to derive analytical results for temperature effects in a relativistic setting [3,22], and we introduce it here for a similar purpose. We thoroughly discuss the relevance of this approximation in our conclusion (Sec. VII). Transverse and parallel temperature will be added in the sequel changing some δ functions to waterbag distributions in f_0^b and f_0^p.

Since our concern is mainly the FIS scenario, the plasma temperature shall not be considered relativistic. Working in the weak beam density limit, one has $V_p=(n_b/n_p)V_b \ll c$, so that only the beam velocity V_b shall eventually be taken relativistic. This simplified calculation for the relativistic factor may be set to 1 in the quadratures involving the plasma distribution function. As for the beam part, we shall set

$$\gamma(\mathbf{p}) = \sqrt{1+\frac{p_x^2+p_y^2+p_z^2}{m_e^2c^2}} \sim \sqrt{1+\frac{p_z^2}{m_e^2c^2}}, \quad (4)$$

which simply means we neglect $(p_x^2+p_y^2)/(m_ec)^2$ due to the nonrelativistic transverse beam motion. Besides, the electromagnetic dispersion equation can be proved [17] to be amenable to the form $P(\mathbf{k},\omega)Q(\mathbf{k},\omega)=0$ with, for the TSF branch ($\eta\equiv\omega/c$),

$$P(\mathbf{k},\omega) = (\eta^2\varepsilon_{xx}-k_z^2)(\eta^2\varepsilon_{zz}-k_x^2)-(\eta^2\varepsilon_{xz}+k_zk_x)^2. \quad (5)$$

The $\varepsilon_{\alpha\beta}$ are the tensor elements given by Eqs. (1). Finally, let us introduce some usual dimensionless variables,

$$\Omega = \frac{\omega}{\omega_p}, \quad \mathbf{Z} = \frac{\mathbf{k}V_b}{\omega_p}, \quad \alpha = \frac{n_b}{n_p}, \quad \beta = \frac{V_b}{c}. \tag{6}$$

Beam and plasma temperature shall be measured through

$$\rho_{b\|} = \frac{V_{tb\|}}{V_b}, \quad \rho_{b\perp} = \frac{V_{tb\perp}}{V_b},$$

$$\rho_{p\|} = \frac{V_{tp\|}}{V_b}, \quad \rho_{p\perp} = \frac{V_{tp\perp}}{V_b}. \tag{7}$$

The beam relativistic factor is $\gamma_b = (1-\beta^2)^{-1/2}$. The beam velocity being the only relativistic velocity of the problem, all the reduced thermal velocities defined above shall be small parameters, which shall be very useful when looking for some asymptotic formulas.

As can be checked in Eq. (2) as well as Eqs. (17), (28), (38), and (46), we model temperature effects through a momentum spread of the beam and plasma distribution functions. The thermal velocities appearing in Eqs. (7) are simply defined from the nonrelativistic momentum spreads through

$$V_{tb\|} = P_{tb\|}/m_e, \quad V_{tb\perp} = P_{tb\perp}/m_e,$$

$$V_{tp\|} = P_{tp\|}/m_e, \quad V_{tp\perp} = P_{tp\perp}/m_e. \tag{8}$$

Having $P_b = \gamma_b m_e V_b$, the parameters ρ's defined by Eqs. (7) read in term of the P_t's

$$\rho_{b\|} = \gamma_b \frac{P_{tb\|}}{P_b}, \quad \rho_{b\perp} = \gamma_b \frac{P_{tb\perp}}{P_b},$$

$$\rho_{p\|} = \gamma_b \frac{P_{tp\|}}{P_b}, \quad \rho_{p\perp} = \gamma_b \frac{P_{tp\perp}}{P_b}. \tag{9}$$

The physical interpretation of $V_{tp\|}, V_{tp\perp}$, and $V_{tb\perp}$ is simple. They represent the physical velocity spread corresponding to the momentum spread used in the distribution functions. The situation is different for $V_{tb\|}$ because the velocity spread corresponding to a momentum spread $P_b \pm P_{tb\|}$ is more involved. Since the beam is relativistic, its parallel velocity spread extends from $V_{b\|}^-$ to $V_{b\|}^+$ with

$$V_{b\|}^- = \frac{P_b - P_{tb\|}}{m_e} \frac{1}{\sqrt{1 + \frac{(P_b - P_{tb\|})^2}{m_e^2 c^2}}},$$

$$V_{b\|}^+ = \frac{P_b + P_{tb\|}}{m_e} \frac{1}{\sqrt{1 + \frac{(P_b + P_{tb\|})^2}{m_e^2 c^2}}}. \tag{10}$$

It is obvious the resulting velocity interval does not read $[V_b - V_{tb\|}, V_b + V_{tb\|}]$ as if V_b were nonrelativistic. Which interpretation can therefore be given to the "thermal velocity" $V_{tb\|} = P_{tb\|}/m_e$ in this setting ? With a nonrelativistic momentum spread ($P_{tb\|} \ll P_b$), the expressions above can be expanded as

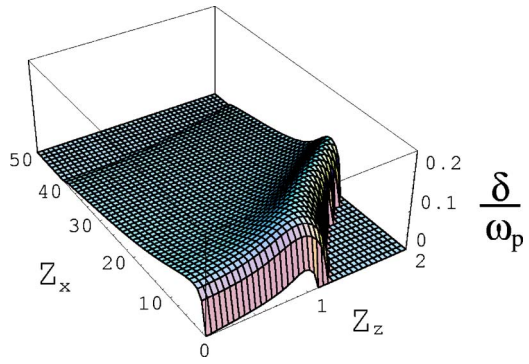

FIG. 1. (Color online) Numerical evaluation of the TSF growth rate for distributions (2) and (3), in terms of $\mathbf{Z} = \mathbf{k}V_b/\omega_p$. Parameters are $\alpha = 0.05$, $\rho_{p\perp} = 0.1$, and $\gamma_b = 4$.

$$V_{b\|}^{\pm} = \frac{P_b}{m_e \gamma_b} \pm \frac{P_{tb\|}}{m_e \gamma_b^3} + O((P_{tb\|}/P_b)^2) = V_b \pm \frac{V_{tb\|}}{\gamma_b^3} + O((P_{tb\|}/P_b)^2). \tag{11}$$

It follows from this equation that a nonrelativistic momentum spread does yield a roughly [28] symmetric velocity spread $\sim V_{tb\|}/\gamma_b^3$ around V_b.

To sum up, let us say that all thermal velocities except $V_{tb\|}$ are real velocity spread. As far as parallel beam thermal spread is concerned, the physical velocity spread would more likely be $\sim V_{tb\|}/\gamma_b^3$ than $V_{tb\|}$, due to the relativistic energy of the beam. This will have non-negligible consequences, as shall be seen in Sec. IV. Finally, even if $V_{tb\|}$ is larger than the real parallel velocity spread by a factor γ^3, the parameter $\rho_{b\|}$ shall still remain small, as can be checked from Eqs. (9), which show that $\rho_{b\|} \sim P_{tb\|}/mc$ (by the way, this is also valid for the three other ρ's).

A typical growth rate map obtained with the distributions (2) and (3) is displayed in Fig. 1. One can easily notice the two oblique features previously mentioned. The maximum growth rate is located away from the main axes and can be approximated through [17]

$$\delta_m^{\mathrm{TSF}} = \frac{\sqrt{3}}{2^{4/3}} \left(\frac{\alpha}{\gamma_b} \right)^{1/3}. \tag{12}$$

Also, the critical angle

$$\theta_c = \arctan\left(\frac{1+\alpha}{\rho_{p\perp}} \right) \tag{13}$$

is evidenced, with an unbounded instability domain in the θ_c direction. Another important property of this angle is that it divides the $\mathbf{k}$ space into a two-stream-like region and a filamentation-like region. Unstable waves are almost longitudinal below this angle while the transition between longitudinal and transverse filamentation waves takes place between θ_c and $\pi/2$. The analysis conducted in [17] shows that as the wave vector departs from the beam axis, the real part of the root yielding the growth rate is located between two singularities. One is located at $\Omega_1 = -\alpha Z \cos\theta_k + Z \sin\theta_k$ and the other at $\Omega_2 = Z\cos\theta_k$. Since $\Omega_1(\theta_k = 0) < \Omega_2(\theta_k = 0)$ while $\Omega_1(\theta_k = \pi/2) > \Omega_2(\theta_k = \pi/2)$, the two singularities necessar-

ily overlap for a given angle, which is precisely the critical angle θ_c. We shall see that the expressions of the singularities may vary with the temperature considered, but the main point is that the instability appears the same way as long as $\Omega_1 < \Omega_2$, defining the two-stream region. We shall even study cases when there is more than one critical angle because singularities are more numerous in the dispersion equation (see Sec. VI for a detailed study). But even in this case, a two-stream region shall still be defined between $\theta_k = 0$ and the smallest critical angle.

While an electromagnetic formalism is required to explore the region beyond θ_c (or beyond the smallest critical angle) up to the filamentation modes at $\pi/2$, the longitudinal approximation with dispersion equation

$$\varepsilon_L(\mathbf{k},\omega) = 0 \tag{14}$$

and

$$\varepsilon_L(\mathbf{k},\omega) = 1 + \frac{4\pi q^2}{k^2} \int \frac{\mathbf{k}\cdot\partial f_0(\mathbf{p})/\partial \mathbf{p}}{\omega - \mathbf{k}\cdot\mathbf{p}/\gamma m} d^3p \tag{15}$$

is a very reliable guide in the two-stream-like region. For example, the longitudinal dispersion equation for the system yielding Fig. 1 reads

$$1 - \frac{1}{(\Omega + \alpha Z_z)^2 - Z_x^2 \rho_{p\perp}^2} - \frac{Z_z^2 + \gamma_b^2 Z_x^2}{Z_z^2 + Z_x^2} \frac{\alpha}{(\Omega - Z_z)^2 \gamma_b^3} = 0, \tag{16}$$

which gives account of the shape of the growth rate "surface" observed in Fig. 1 for small enough values of Z_x.

III. TRANSVERSE BEAM TEMPERATURE EFFECTS

Adding a temperature in the system consists in adding an electron population to the beam or the plasma with a special orientation. One can think in terms of the Dawson model [23] where every distribution is considered as the superposition of cold beams. Transverse beam temperature, for example, adds some beam electrons having a velocity with a component normal to the beam. Since two-stream longitudinal modes have their wave vector and their electric field aligned with the beam, it is expected that they interact poorly with transverse thermal beam electrons. On the other hand, transverse beam temperature effect has been found to be very strong on filamentation instability [3] so that one may ask when the influence starts as the angle θ_k increases. We now shall investigate quantitatively this temperature effect replacing distribution function (3) for the electron beam by

$$f_0^b = \frac{n_b}{(2P_{tb\perp})^2}[\Theta(p_x + P_{tb\perp}) - \Theta(p_x - P_{tb\perp})] \times [\Theta(p_y + P_{tb\perp}) - \Theta(p_y - P_{tb\perp})]\delta(p_z - P_b). \tag{17}$$

A. Two-stream instability

We set here $k_x = 0$ in Eqs. (1) and (5). Calculation of the dispersion equation for the TSF branch is straightforward and one obtains the well-known dispersion equation

$$1 - \frac{1}{(\Omega + \alpha Z_z)^2} - \frac{\alpha}{(\Omega - Z_z)^2 \gamma_b^3} = 0, \tag{18}$$

which bears no transverse beam temperature effect. In the limit $\alpha \ll 1$, modes are unstable for $Z_z < 1 + (3/2)\alpha^{1/3}/\gamma_b$. The maximum growth rate

$$\delta_{m0}^{TS} = \frac{\sqrt{3}}{2^{4/3}} \frac{\alpha^{1/3}}{\gamma_b} \tag{19}$$

is reached for $Z_z \sim 1$ and is free of any transverse beam temperature effect. We now derive the maximum growth rate (19) following the resolution method of Mikhailovskii [24]. The method is explained here and used in Secs. IV and V. We start by noting that since the beam is considered as a perturbation ($\alpha \ll 1$), solutions of the dispersion equation are to be found near $\Omega = 1$. We therefore set $\Omega = 1 + \delta$ and look for solutions of

$$1 - \frac{1}{(1 + \delta + \alpha Z_z)^2} - \frac{\alpha}{(1 - Z_z + \delta)^2 \gamma_b^3} = 0. \tag{20}$$

The unstable modes are perturbations of the proper waves of the plasma without beam so that $\omega \sim \omega_p$. The maximum growth rate is therefore found for $Z_z = k_z V_b/\omega_p \sim 1$ so that the coupling between the wave and the beam electrons is maximal ($k/\omega \sim k/\omega_p \sim V_b$). We assume both $|\delta| \gg \alpha$ and $1 - Z_z \ll \delta$. This allows us to rewrite Eq. (20) as

$$1 - (1 - 2\delta) - \frac{\alpha}{\delta^2 \gamma_b^3} = 0, \tag{21}$$

which is easily solved and yields the growth rate (19) as the imaginary part of

$$\Omega_{TS} = 1 - \frac{1}{2^{4/3}} \frac{\alpha^{1/3}}{\gamma_b} + i \frac{\sqrt{3}}{2^{4/3}} \frac{\alpha^{1/3}}{\gamma_b}. \tag{22}$$

Coming back to the assumption $|\delta| \gg \alpha$, we now see it implies $\gamma_b \alpha^{2/3} \ll 1$.

B. Filamentation instability

We consider here a wave vector normal to the beam. We set $k_z = 0$ in Eqs. (1) and (5) and derive the dispersion equation by setting $\rho_{p\parallel} = 0$ in Eq. (A1) reproduced in the Appendix. The numerator of the resulting expression appears to be an even polynomial which can only have two conjugated purely imaginary roots. In the limits $\alpha, \rho_{p\perp} \ll 1$ and $\rho_{b\perp}/\rho_{p\perp} \ll 1$, modes are unstable for

$$Z_x \lesssim \frac{\beta\gamma_b}{\rho_{p\perp}} \left(1 - \frac{\gamma_b^3}{2\alpha} \frac{\rho_{b\perp}^2}{\rho_{p\perp}^2}\right), \tag{23}$$

which shows that the instability domain is drastically reduced as soon as $\rho_{b\perp} > 0$. The maximum growth rate is fairly well fitted by

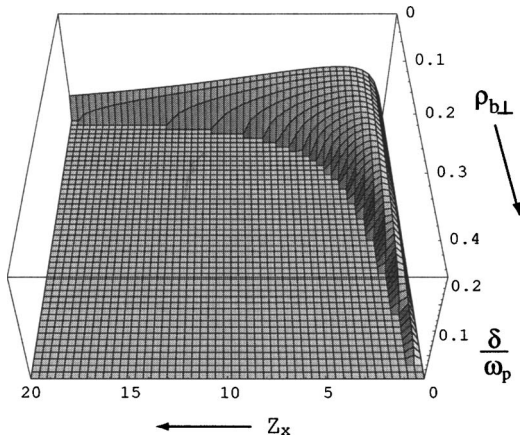

FIG. 2. (Color online) Filamentation growth rate as a function of Z_x and beam transverse temperature $\rho_{b\perp}$. The instability domain dramatically shrinks as soon as $\rho_{b\perp}>0$. Parameters are $\alpha=0.05$, $\gamma_b=4$, and $\rho_{p\perp}=0.1$. The instability vanishes for $\rho_{b\perp}\sim\sqrt{\alpha\gamma_b}=0.44$.

$$\delta_m^F \sim \beta\sqrt{\frac{\alpha}{\gamma_b}}\left(1-\frac{\rho_{b\perp}^2}{\alpha\gamma_b}\right), \tag{24}$$

so that the instability vanishes for $\rho_{b\perp}\sim\sqrt{\alpha\gamma_b}$. The well-known stabilizing effect of the beam temperature is thus recovered. Stabilization is achieved both by the reduction of the instability domain [see Eq. (23)] and by the reduction of the maximum growth rate [see Eq. (24)]. Even if the latter is less efficient than the former, total suppression of the instability can still be achieved for a nonrelativistic transverse beam temperature. Figure 2 shows a numerical evaluation of the growth rate in terms of Z_x and $\rho_{b\perp}$ and we recover the results of Silva *et al.* [3].

C. Arbitrary wave-vector orientation

We found no beam transverse temperature correction to the two-stream configuration, while those effects are important for filamentation. Our goal from now on is to find out when transverse beam temperature becomes an important factor as the wave vector departs from the beam axis.

The singularities of the dispersion function $P(\mathbf{k},\omega)$ defined by Eq. (5) play a key role in the behavior of the dispersion equation solutions. For a cold relativistic beam and a transversely hot plasma, they can be written in terms of the dimensionless variables (6) and (7) as [17]

$$\Omega_1 = -Z\alpha\cos\theta_{\mathbf{k}} - Z\rho_{p\perp}\sin\theta_{\mathbf{k}},$$

$$\Omega_2 = -Z\alpha\cos\theta_{\mathbf{k}} + Z\rho_{p\perp}\sin\theta_{\mathbf{k}},$$

$$\Omega_3 = Z\cos\theta_{\mathbf{k}}. \tag{25}$$

When adding a transverse temperature to the beam, they read

$$\Omega_1 = -Z\alpha\cos\theta_{\mathbf{k}} - Z\rho_{p\perp}\sin\theta_{\mathbf{k}},$$

$$\Omega_2 = -Z\alpha\cos\theta_{\mathbf{k}} + Z\rho_{p\perp}\sin\theta_{\mathbf{k}},$$

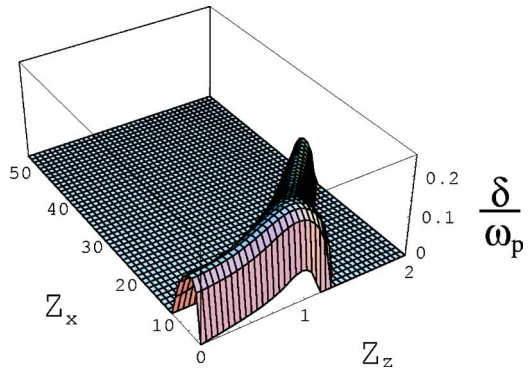

FIG. 3. (Color online) Full electromagnetic evaluation of the growth rate for the TSF branch in terms of $\mathbf{Z}=\mathbf{k}V_b/\omega_p$ for a transversely hot REB. Parameters are $\alpha=0.05$, $\gamma_b=4$, $\rho_{p\perp}=0.1$, and $\rho_{b\perp}=0.1$.

$$\Omega_3 = Z\cos\theta_{\mathbf{k}} - Z\frac{\rho_{b\perp}}{\gamma_b}\sin\theta_{\mathbf{k}},$$

$$\Omega_4 = Z\cos\theta_{\mathbf{k}} + Z\frac{\rho_{b\perp}}{\gamma_b}\sin\theta_{\mathbf{k}}. \tag{26}$$

From an analytical point of view, beam temperature splits the Ω_3 singularity of Eqs. (25) into the Ω_3 and Ω_4 singularities of Eqs. (26). When $\theta_{\mathbf{k}}=0$, one has $\Omega_1=\Omega_2$ and $\Omega_3=\Omega_4$, and the root of the dispersion equation corresponding to the two-stream instability has its real part between the two singularities. The analysis is eventually identical to the one conducted for the cold beam case [17] except that one must take the Ω_3 singularity value from Eqs. (26) rather than from Eqs. (25). The identity $\Omega_2=\Omega_3$ yields the new critical angle value

$$\theta_c = \arctan\left(\frac{1+\alpha}{\rho_{p\perp}+\rho_{b\perp}/\gamma_b}\right). \tag{27}$$

The evaluation of the growth rate all over the (Z_x,Z_z) plane displayed in Fig. 3 unravels how exactly transverse beam temperature effect switches from possible suppression along the normal direction to no effect at all along the parallel direction: the "frontier" appears to be the critical angle θ_c. Modes with wave vector below the critical angle are almost unaffected (compare Fig. 3 with Fig. 1), whereas those situated beyond are much less unstable.

The ratio between the maximum growth rate numerically calculated and the analytical formula (12) is plotted in Fig. 4 in terms of the beam temperature $\rho_{b\perp}$. The agreement is good in the nonrelativistic temperature domain $\rho_{b\perp}\ll 1$ (since $V_b\sim c$) considered here, although a slight stabilization is observed for $\rho_{b\perp}>0.01$. Unlike the filamentation instability, which can be perfectly suppressed by a nonrelativistic transverse beam temperature (with $\alpha=10^{-3}$ and $\gamma_b=4$, filamentation instability vanishes for $\rho_{b\perp}\sim 0.06$), our calculations show that a nonrelativistic transverse beam temperature shall not significantly damp the most unstable mode.

An interesting consequence of this "selective stabilization" has to do with the validity of the longitudinal approximation. Indeed, this approximation fails precisely where

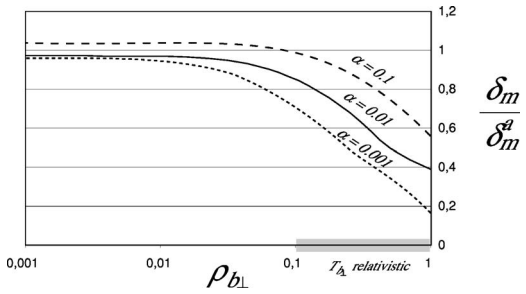

FIG. 4. Ratio between the numerical evaluation δ_m of the maximum growth rate and the analytical formula δ_m^a [Eq. (12)] in terms of the beam transverse temperature for $\alpha=0.1$, 0.01, and 0.001 ($\gamma_b=4$ and $\rho_{p\perp}=0.1$). Those calculations are valid for $\rho_{b\perp}\ll 1$.

transverse beam temperature lowers the growth rate. It can therefore be said that it is even more reliable in this case, since growth rate tends to vanish where it already yields stable modes.

IV. PARALLEL BEAM TEMPERATURE EFFECTS

We now replace the beam distribution function (3) for the electron beam by

$$f_0^b = \frac{n_b}{2P_{tb\|}}\delta(p_x)\delta(p_y) \times [\Theta(p_z - P_b + P_{tb\|}) - \Theta(p_z - P_b - P_{tb\|})], \tag{28}$$

leaving distribution function (2) unchanged.

A. Two-stream instability

The dispersion equation found here for the two-stream instability is

$$1 - \frac{1}{(\Omega + \alpha Z_z)^2} - \frac{\alpha}{2Z_z\rho_{b\|}}\left(\frac{1}{\Omega - Z_z\Gamma_b^+} - \frac{1}{\Omega - Z_z\Gamma_b^-}\right) = 0, \tag{29}$$

with

$$\Gamma_b^\pm = \frac{\gamma_b \pm \rho_{b\|}}{\sqrt{1+\beta^2(\gamma_b \pm \rho_{b\|})^2}}. \tag{30}$$

The beam part can be simplified for $\rho_{b\|}\ll\gamma_b$, a condition very easily fulfilled in our case, and reads then

$$0 = 1 - \frac{1}{(\Omega + \alpha Z_z)^2} - \frac{\alpha/\gamma_b^3}{(\Omega - Z_z)^2 - (Z_z\rho_{b\|}/\gamma_b^3)^2}. \tag{31}$$

The resolution method presented in Sec. III A can be applied, yielding the very same growth rate, providing a condition we shall determine here is fulfilled. Looking for the maximum growth rate with $\Omega = 1+\delta$ and $Z_z \sim 1$, we can apply the same method and solve the dispersion equation the same way as long as $|\delta| \gg \rho_{b\|}/\gamma_b^3$. Since δ is a complex number with $|\delta| \sim \alpha^{1/3}/\gamma_b$, this means that parallel beam temperature may be neglected in the two-stream instability as long as

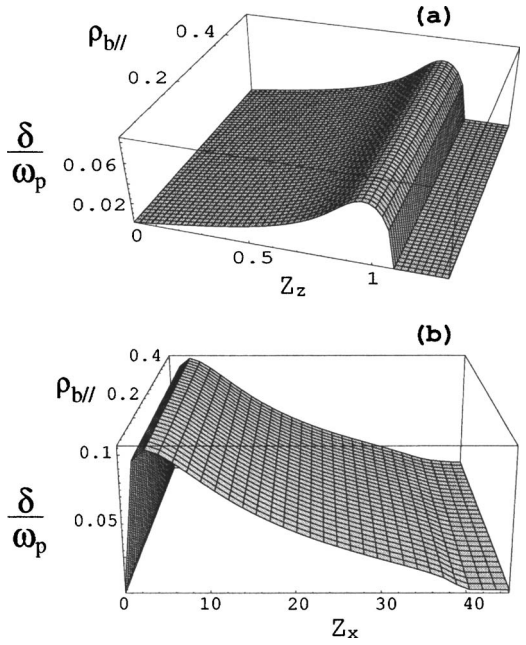

FIG. 5. (Color online) Influence of the parallel beam temperature on the two-stream instability (a) and filamentation instability (b). Parameters are $\alpha=0.05$ and $\gamma_b=4$.

$$\rho_{b\|} \ll \alpha^{1/3}\gamma_b^2 \Leftrightarrow \frac{\rho_{b\|}^3}{\gamma_b^6} \ll \alpha(\ll 1). \tag{32}$$

When beam temperature exceeds this threshold, it is known [24] that the growth rate eventually behaves as $\alpha/\rho_{b\|}^2$ instead of $\alpha^{1/3}$ while the maximum growth rate is reached for [25]

$$Z \sim \frac{1}{1 - \rho_{b\|}/\gamma_b^3}. \tag{33}$$

It is noticeable that condition (32) is very easily fulfilled. Actually, for a beam with $\gamma_b=4$ and α even as small as 10^{-4}, one finds that parallel beam temperature can be neglected when $\rho_{b\|}\ll 0.74$, which just means a nonrelativistic temperature since $V_b \sim c$. The solution is to be found in the velocity dispersion corresponding to a given momentum dispersion in the distribution function. For a nonrelativistic beam, a thermal momentum spread $\pm P_{tb\|}$ around the beam momentum P_b yields a velocity spread $\pm P_{tb\|}/m$. But this simple picture can no longer hold for a relativistic beam velocity since $V_b \sim c$ forbids any significative thermal spread above V_b. Indeed, the same nonrelativistic momentum spread $\pm P_{tb\|}$ yields now a velocity spread $\sim \pm P_{tb\|}/m\gamma_b^3$ so that relativistic effects dramatically shrink the velocity spread corresponding to the same momentum spread, and this all the more than V_b is approaching c. The instability, which relies on wave-particle resonance and tends to be reduced through thermal *velocity* spread, is here very weakly affected, whereas effects are much more pronounced in the nonrelativistic regime [24]. The two-stream instability profile is plotted in Fig. 5(a) in terms of Z_z and $\rho_{b\|}$ with such parameters, and one can check that parallel beam temperature hardly affects it.

B. Filamentation instability

Dispersion equation obtained for the filamentation instability is too large to be reproduced here. Suffice it to say that its nonrelativistic counterpart only differs from the cold beam version by the beam element ε_{zz}^{b} of the dielectric tensor with

$$\varepsilon_{zz}^{b} = -\alpha \frac{\Omega^2 + Z_x^2(1+\rho_{b\|}^2/3)}{\Omega^4}. \tag{34}$$

Transverse beam temperature influence is therefore very weak in the nonrelativistic thermal regime $\rho_{b\|} \ll 1$. Figure 5(b) shows the same behavior for the relativistic case even for high values of $\rho_{b\|}$, although a slight enhancement of the instability domain is observed.

C. Arbitrary wave-vector orientation

From what we just saw regarding the two-stream and the filamentation instabilities, stability properties are two-stream-like below θ_c and filamentation-like beyond it. The critical angle analysis starts with the singularities of the dispersion equation. In the present case, they are

$$\Omega_1 = -Z\alpha \cos\theta_{\mathbf{k}} - Z\rho_{p\perp}\sin\theta_{\mathbf{k}},$$

$$\Omega_2 = -Z\alpha \cos\theta_{\mathbf{k}} + Z\rho_{p\perp}\sin\theta_{\mathbf{k}},$$

$$\Omega_3 = Z\Gamma_b^{-}\cos\theta_{\mathbf{k}},$$

$$\Omega_4 = Z\Gamma_b^{+}\cos\theta_{\mathbf{k}}, \tag{35}$$

where the $\Gamma_b^{\pm}$ are given by Eq. (30). Quantities $\Omega_{3,4}$ can be very well approximated $(\rho_{b\|}/\gamma_b^3 \ll 1)$ by

$$\Omega_3 = Z\cos\theta_{\mathbf{k}} - Z\frac{\rho_{b\|}}{\gamma_b^3}\cos\theta_{\mathbf{k}},$$

$$\Omega_4 = Z\cos\theta_{\mathbf{k}} + Z\frac{\rho_{b\|}}{\gamma_b^3}\cos\theta_{\mathbf{k}}. \tag{36}$$

The critical angle is now defined by the overlapping of singularities Ω_2 and Ω_3 and reads

$$\theta_c = \arctan\left(\frac{1+\alpha-\rho_{b\|}/\gamma_b^3}{\rho_{p\perp}}\right). \tag{37}$$

The growth rate for the full TSF branch is plotted in Fig. 6 and confirms what was expected. Parallel beam temperature eventually poorly affects the TSF growth rate. Noting that the change in the critical angle is very small, we can conclude that the overall effect of parallel beam temperature is negligible in the nonrelativistic temperature regime.

V. PARALLEL PLASMA TEMPERATURE EFFECTS

We finally consider a plasma with temperature in every direction. This will enable us to probe the important case of the isotropic plasma [29]. We therefore replace the plasma distribution function (2) by

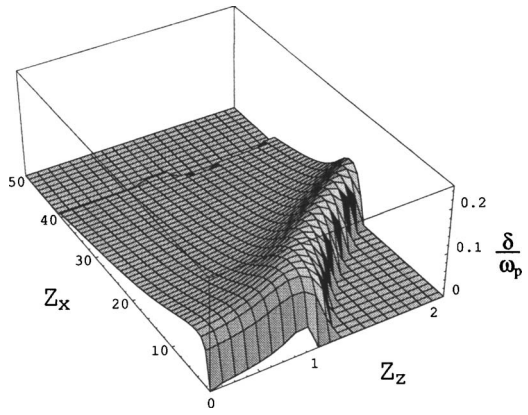

FIG. 6. (Color online) Influence of the parallel beam temperature on the full TSF branch. Parameters are $\alpha=0.05$, $\gamma_b=4$, and $\rho_{b\|}=0.4$.

$$f_0^p = \frac{n_p}{(2P_{tp\perp})^2 2P_{tp\|}}[\Theta(p_x+P_{tp\perp})-\Theta(p_x-P_{tp\perp})] \times [\Theta(p_y+P_{tp\perp})-\Theta(p_y-P_{tp\perp})] \times [\Theta(p_z+P_{tp\|}+P_p)-\Theta(p_z-P_{tp\|}+P_p)]. \tag{38}$$

Here is added to the system an electron population with velocity centered around the return current. Since the phase velocity of the mode leading to the maximum two-stream growth rate is V_b, this new electron population is expected to interact poorly with the most unstable two-stream mode. From a mathematical point of view, changes in the dispersion function are localized around $\Omega=-\alpha Z_z$ while the root with higher imaginary part is found around $\Omega=Z_z$. Nevertheless, effects should increase on the TSF branch as we approach filamentation modes since their phase velocity vanishes. As a summary, the effect of parallel plasma temperature is expected to be weak in the two-stream region while stronger near filamentation, the border between the two regions being delimited by the angle θ_c.

A. Two-stream instability

The dispersion equation found here for the two-stream instability is

$$1 - \frac{1}{(\Omega+\alpha Z_z)^2 - (Z_z\rho_{p\|})^2} - \frac{\alpha}{(\Omega-Z_z)^2\gamma_b^3} = 0. \tag{39}$$

One readily sees the equation is slightly affected as long as $\rho_{p\|} \ll 1$. Setting $\Omega=1+\delta$, the resolution method presented in Sec. III A can be applied if $\delta \gg \alpha+\rho_{p\|}$, which is slightly stronger than $\delta \gg \alpha$ for a nonrelativistic temperature. However, Fig. 7(a) displays a plot of the two-stream profile for values of $\rho_{p\|}$ up to 0.5 and one can check that the overall $\rho_{p\|}$ influence is weak even for $\alpha=10^{-3}$, although a small shift of the maximum growth rate is observed. This weak $\rho_{p\|}$ dependence can be understood noticing $\rho_{p\|}$ only appears as a second-order quantity in the dispersion equation whereas α is present at first order.

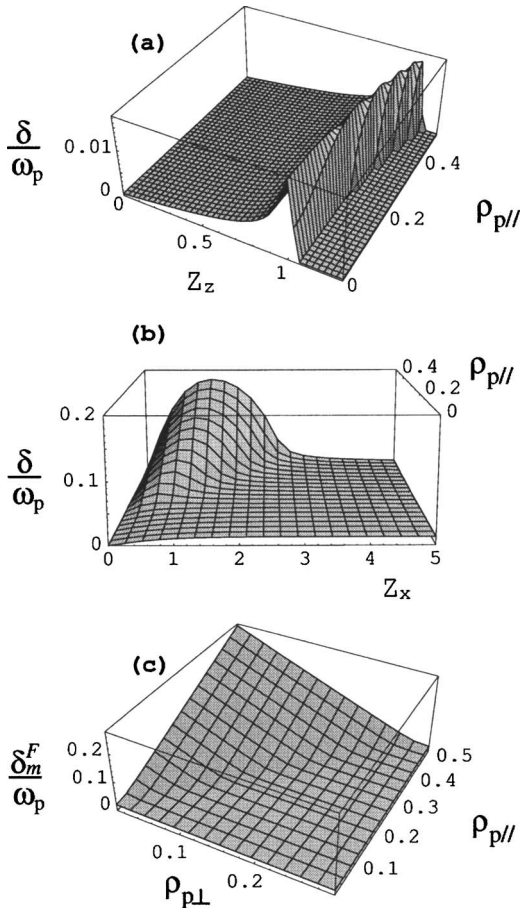

FIG. 7. (Color online) Influence of the parallel plasma temperature on the two-stream instability (a) and the filamentation instability (b). (c) Maximum filamentation growth rate in terms of $\rho_{p\perp}$ and $\rho_{p\|}$. Parameters are $\alpha=10^{-3}$ and $\gamma_b=4$ for all figures and $\rho_{p\perp}=0.1$ for (a) and (b).

B. Filamentation instability

As for the filamentation instability when parallel beam temperature is introduced, the only change in the dispersion equation appears in the plasma dielectric tensor element ε_{zz}^p with

$$\varepsilon_{zz}^p = -\frac{\Omega^2 + Z_x^2(\alpha^2 - \rho_{p\perp}^2 + \rho_{p\|}^2/3)}{\Omega^4 - \Omega^2 Z_x^2 \rho_{p\perp}^2}. \tag{40}$$

The situation is more involved than it was when we added a parallel temperature to the beam because the three quantities $\alpha^2, \rho_{p\perp}^2$, and $\rho_{p\|}^2/3$ have the same order of magnitude. Nevertheless, it can be said straightforwardly that parallel plasma temperature is negligible when

$$\rho_{p\|} \ll \sqrt{3}\rho_{p\perp}. \tag{41}$$

A plasma with a temperature anisotropy fulfilling this condition can therefore be considered as cold in the parallel direction (at least as far as filamentation instability is concerned).

Increasing $\rho_{p\|}/\rho_{p\perp}$, we encounter the isotropic plasma with $\rho_{p\|}=\rho_{p\perp}=\rho_p$. For such a situation, we develop around $\Omega=0$ the dispersion equation and search under which conditions (on α, ρ_p, and γ_b) the zeroth-order term vanishes. This tells us when filamentation instability vanishes. It is found that in the limit $\alpha \ll 1$, the filamentation instability vanishes for $\rho_p \sim \sqrt{3/2}$. This does not make sense physically, but the maximum growth rate is very well fitted by

$$\delta_m^F \sim \beta\sqrt{\frac{\alpha}{\gamma_b}}\left(1 - \frac{\rho_p}{\sqrt{3/2}}\right), \tag{42}$$

which results in a slight reduction of the instability.

If we keep on increasing plasma parallel temperature, we reach the opposite regime to Eq. (41), namely strong plasma temperature anisotropy with $\rho_{p\|} \gg \sqrt{3}\rho_{p\perp}$. Studying the regime $\rho_{p\|} \gg \sqrt{3}\rho_{p\perp}$ (through $\rho_{p\perp}=0$ and with the same method mentioned above) yields the maximum growth rate,

$$\delta_m^F \sim \beta\sqrt{\frac{\alpha}{\gamma_b}}\sqrt{1 + \frac{\gamma_b}{3\alpha}\rho_{p\|}^2}. \tag{43}$$

Filamentation growth rate is thus very boosted by plasma parallel temperature, as displayed in Fig. 7(b). In order to clearly evidence this growth rate boosting with plasma temperature, we have plotted the numerical evaluation of δ_m^F as a function of $\rho_{p\perp}$ and $\rho_{p\|}$ in Fig. 7(c). The increase with $\rho_{p\|}$ is obvious, together with the border $\rho_{p\|}=\sqrt{3}\rho_{p\perp}$ under which one can set parallel plasma temperature to zero.

Though our temperature review is not finished yet, let us say from now that we are witnessing here one of the strongest temperature effects, together with the transverse beam temperature effect on the same instability. Among all the beam/plasma/transverse/parallel temperature effects upon the two-stream/filamentation instabilities, the only "couples" we found bearing significant nonrelativistic temperature corrections are ($\rho_{b\perp}$, filamentation) and ($\rho_{p\|}$, filamentation). But unlike the other "couples," which result in a reduction of the instability, this one is found to produce the opposite. We shall study more in detail in Sec. VI how the couple "transverse beam temperature/parallel plasma temperature" eventually affects the filamentation instability.

One may think this filamentation instability boosting under plasma temperature anisotropy is nothing more than the "original" anisotropy driven Weibel instability. The modes we are studying are purely transverse, as are the Weibel ones, and seem to arise from some plasma temperature anisotropy. Indeed, rewriting Eq. (43) when $\gamma_b\rho_{p\|}^2/3\alpha \gg 1$ yields $\delta_m^F \sim \beta\rho_{p\|}/\sqrt{3}$, which is exactly the Weibel growth rate found in the waterbag model [17]. Furthermore, this quantity does not depend on the beam (no α), which is the signature of the Weibel instability. What we found here is a continuous transition between filamentation and Weibel modes, with, as in [2], a wave vector normal to the high-temperature axis. This leads us to the very interesting conclusion that one single unstable eingenmode switches continuously between the two-stream, the filamentation, and the Weibel instabilities through the interplay of wave-vector orientation ($\theta_k=0 \rightarrow \pi/2$) and plasma parallel and normal temperature ($\rho_{p\|}/\rho_{p\perp}=1 \rightarrow \infty$). Although the first two are "beam based" whereas the latter is "plasma temperature based," they all can be recovered from the same branch of the electromagnetic dispersion equation $P(\mathbf{k},\omega)=0$ [see Eq. (5)]. We shall in the

sequel refer to this mode as the filamentation/Weibel instability. Let us restate for clarity that we mean here an intermediate mode between the beam driven filamentation instability and the plasma anisotropy driven Weibel instability. We close this discussion noting that if the plasma temperature anisotropy is inverted, that is if $\rho_{p\parallel}/\rho_{p\perp} \to 0$, the resulting Weibel instability appears on the other branch, $Q(\mathbf{k},\omega)=0$, with a wave vector aligned with the z axis [17].

C. Arbitrary wave-vector orientation

The singularities of the dispersion equation are now

$$\Omega_1 = -Z\alpha\cos\theta_{\mathbf{k}} - Z\rho_{p\perp}\sin\theta_{\mathbf{k}} - Z\rho_{p\parallel}\cos\theta_{\mathbf{k}},$$

$$\Omega_2 = -Z\alpha\cos\theta_{\mathbf{k}} - Z\rho_{p\perp}\sin\theta_{\mathbf{k}} + Z\rho_{p\parallel}\cos\theta_{\mathbf{k}},$$

$$\Omega_3 = -Z\alpha\cos\theta_{\mathbf{k}} + Z\rho_{p\perp}\sin\theta_{\mathbf{k}} - Z\rho_{p\parallel}\cos\theta_{\mathbf{k}},$$

$$\Omega_4 = -Z\alpha\cos\theta_{\mathbf{k}} + Z\rho_{p\perp}\sin\theta_{\mathbf{k}} + Z\rho_{p\parallel}\cos\theta_{\mathbf{k}},$$

$$\Omega_5 = Z\cos\theta_{\mathbf{k}}. \tag{44}$$

One may check that for $\theta_k=0$ one has $\Omega_{1234}<\Omega_5$, whereas for $\theta_k=\pi/2$ one has $\Omega_{34}>\Omega_5$. We therefore recover two critical angles θ_{c1} and θ_{c2} (see the general analysis in Sec. VI) which correspond to the angles where $\Omega_5=\Omega_4$ and $\Omega_5=\Omega_3$,

$$\theta_{c12} = \arctan\left(\frac{1+\alpha \mp \rho_{p\parallel}}{\rho_{p\perp}}\right), \tag{45}$$

where the "–" stands for θ_{c1} and the "+" for θ_{c2}. Instead of one critical angle, we now have two defined by Eqs. (45). These two angles are very close to each other with $\tan\theta_{c12} \sim 1/\rho_{p\perp}$ and both define a direction in which the growth rate remains important at high $Z=kV_b/\omega$. Figures 8(a) and 8(b) display the growth rate for the TSF branch for an isotropic (a) and an anisotropic (b) plasma. For an isotropic plasma with $\rho_p=0.1$, the only noticeable difference with our basic model (Fig. 1) is found on the "ridge" in the critical angle directions, where a slight depression is observed. This slight depression corresponds to angles comprised between θ_{c1} and θ_{c2}. Whether the instability domain is bounded in these directions is quite difficult to prove analytically, although numerical exploration conducted for high values of Z tends to prove it is. For the anisotropic plasma with $\rho_{p\parallel}=0.3$ and $\rho_{p\perp}=0.05$, the two critical angles are obvious in Fig. 8(b), together with the filamentation transition to the Weibel regime. Indeed, the maximum growth rate all over the TSF may now be the filamentation/Weibel one. Comparing this filamentation/Weibel growth rate $\delta_m^{\mathrm{FW}} \sim \beta\rho_{p\parallel}/\sqrt{3}$ with Eq. (12) for δ_m^{TSF}, we find δ_m^{FW} shall exceed δ_m^{TSF} in low plasma density and high γ_b beam. Yet, many conditions are required to find the maximum growth rate on the Z_x axis: strong plasma temperature anisotropy, very low beam density, and (or) high γ_b. The situation we have just studied is therefore very interesting with the smooth transition between filamentation and the Weibel regime, but one can still say the maximum growth rate shall generally be found off axis [5], and

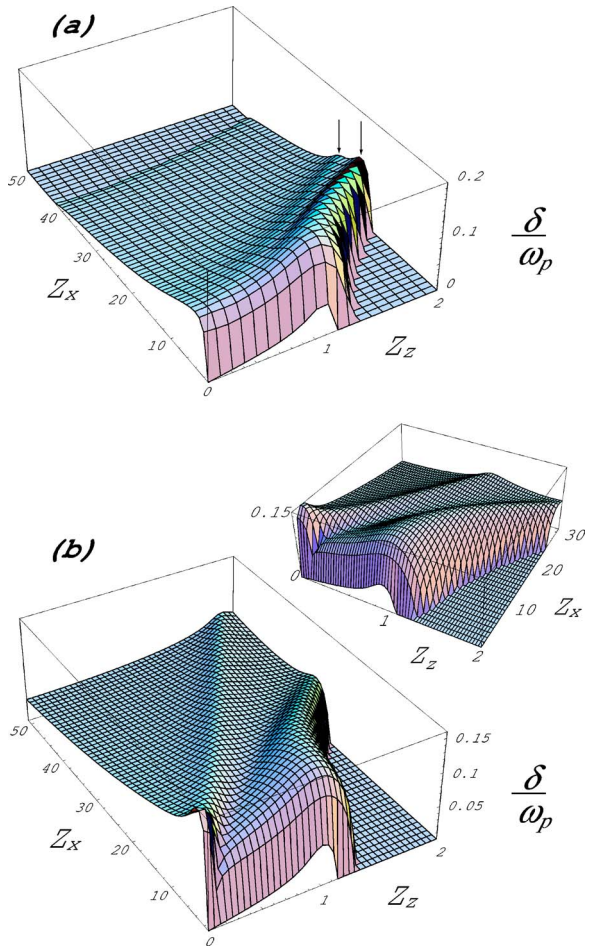

FIG. 8. (Color online) Influence of the parallel plasma temperature on the whole TSF branch for an isotropic plasma (a) and an anisotropic plasma (b). Parameters are $\alpha=0.05$ and $\gamma_b=4$ for both figures. Temperatures are $\rho_p=0.1$ in (a) and $\rho_{p\parallel}=0.3$ and $\rho_{p\perp}=0.05$ in (b). The arrows on (a) show the direction of the two critical angles and (b) is displayed from two points of view for a better appreciation of the filamentation amplification.

all the more when accounting for transverse beam temperature, which can suppress the filamentation instability but not the maximum TSF growth rate. The overall influence of temperatures acting together will be studied in the last part (Sec. VI).

VI. FULL PLASMA AND BEAM TEMPERATURE EFFECTS

We finally look at the behavior of the system when all temperatures are accounted for using the distribution functions

$$f_0^p = \frac{n_p}{(2P_{tp\perp})^2 2P_{tp\parallel}}[\Theta(p_x+P_{tp\perp})-\Theta(p_x-P_{tp\perp})]$$
$$\times[\Theta(p_y+P_{tp\perp})-\Theta(p_y-P_{tp\perp})]$$
$$\times[\Theta(p_z+P_{tp\parallel}+P_p)-\Theta(p_z-P_{tp\parallel}+P_p)],$$

$$f_0^b = \frac{n_b}{(2P_{tb\perp})^2 2P_{tb\parallel}}[\Theta(p_x + P_{tb\perp}) - \Theta(p_x - P_{tb\perp})] \times [\Theta(p_y + P_{tb\perp}) - \Theta(p_y - P_{tb\perp})] \times [\Theta(p_z + P_{tb\parallel} - P_b) - \Theta(p_z - P_{tb\parallel} - P_b)]. \quad (46)$$

We shall not spend much time discussing the two-stream instability since we saw in previous sections that as long as temperatures are nonrelativistic, none significantly affects its growth rate. On the other hand, temperature effects on filamentation instability are numerous and we shall now devote a section to their investigation.

A. Filamentation instability

As far as filamentation instability is concerned, we noticed a reduction from transverse beam temperature as well as an amplification from parallel plasma temperature through a filamentation/Weibel transition. It is then worthwhile to investigate the effect of these two temperatures joined together.

For the isotropic plasma with temperatures $\rho_{p\perp}=\rho_{p\parallel}=\rho_p$, we find that transverse beam temperature reduces the instability and eventually suppresses it for

$$\rho_{b\perp} \gtrsim \sqrt{\frac{3\alpha\gamma_b}{2}}\sqrt{1-\frac{2\rho_p^2}{3}}, \quad (47)$$

so that the cancellation threshold slightly decreases with plasma temperature. The important point is that there is still a threshold for the cancellation of the instability through transverse beam temperature. We shall see now that this is not always the case.

We now turn to the anisotropic plasma and the interesting interplay between parallel plasma temperature enhancement and normal beam temperature reduction of the filamentation/Weibel instability [30]. We shall mainly focus here on the maximum growth rate and the reason for it after Figs. 9(a)–9(d), where we have plotted the maximum filamentation growth rate in terms of $\rho_{p\parallel}$ and $\rho_{b\perp}$ for various plasma normal temperatures. It can be seen that the maximum filamentation growth rate is always reached for $\rho_{b\perp}=0$, where it can be evaluated through Eq. (43) as long as $\rho_{p\perp} \ll \rho_{p\parallel}/\sqrt{3}$. When normal plasma temperature increases, one sees that the maximum growth rate dependence on $\rho_{p\parallel}$ weakens. As transverse plasma temperature increases [Figs. 9(b)–9(d)], filamentation is less and less "Weibel-like," and one can say the growth rate always remains smaller than the value it reaches for $\rho_{p\parallel}=0$ and $\rho_{b\perp}=0$, namely $\beta\sqrt{\alpha/\gamma_b}$, which is the typical filamentation growth rate. Indeed, it can be checked in Figs. 9(c) and 9(d) that the maximum growth rate reached for $\rho_{b\perp}=0$ is almost constant and does not depend on $\rho_{p\parallel}$ and $\rho_{p\perp}$. The stabilizing effects of transverse beam temperature is retrieved in all figures, although complete suppression demands more and more transverse beam temperature to be achieved as transverse plasma temperature increases. Concerning the value of $\rho_{b\perp}$ necessary to cancel the instability, one needs $\rho_{b\perp} \sim \sqrt{\alpha\gamma_b}$ when $\rho_{p\parallel}=0$. This threshold increases with $\rho_{p\parallel}$ according to

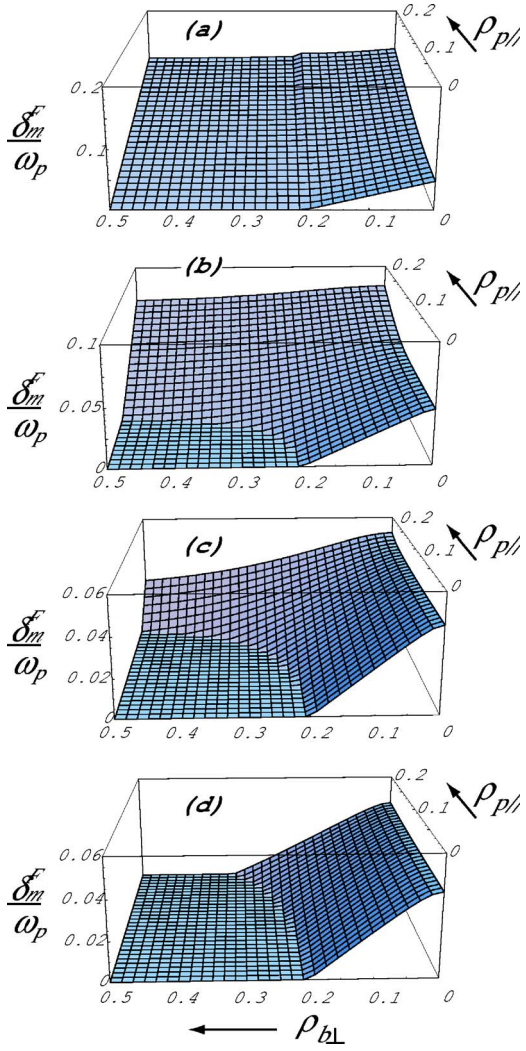

FIG. 9. (Color online) Interplay of parallel plasma temperature vs transverse beam temperature upon the maximum growth rate of the filamentation instability. Parameters are $\alpha=0.01$, $\gamma_b=4$, and (a) $\rho_{p\perp}=0$, (b) $\rho_{p\perp}=0.05$, (c) $\rho_{p\perp}=0.1$, and (d) $\rho_{p\perp}=0.15$.

$$\rho_{b\perp} > \frac{\sqrt{\alpha\gamma_b}}{\sqrt{1-\rho_{p\parallel}^2/3\rho_{p\perp}^2}}. \quad (48)$$

As long as $\rho_{p\parallel}/\rho_{p\perp} \ll 1$, we recover the stabilizing effect of transverse beam temperature. But as Eq. (48) makes it clear, and Figs. 9(b) and 9(c) suggest strongly, there is a limit value of $\rho_{p\parallel}$ beyond which transverse beam temperature can no longer stabilize filamentation. It is straightforward from Eq. (48) that this critical value of $\rho_{p\parallel}$ is $\sqrt{3}\rho_{p\perp}$, a quantity which we already encountered in Sec. V. The anisotropy threshold of $\rho_{p\parallel}/\rho_{p\perp}=\sqrt{3}$ corresponds to the transition to the Weibel regime, when the instability is no longer "beam based" but "plasma temperature anisotropy based." What we check here is that this threshold does not depend on beam temperature, which may not be surprising since we are dealing precisely with a transition to a regime independent of the beam. This discussion can be summed up very simply: As long as $\rho_{p\parallel} < \sqrt{3}\rho_{p\perp}$, the instability is filamentation-like and can be reduced through transverse beam temperature. When $\rho_{p\parallel}$

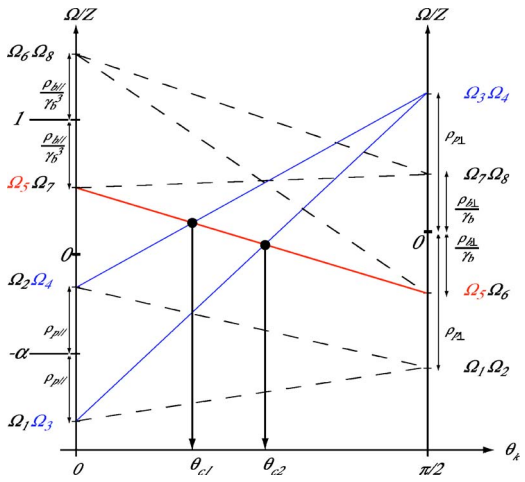

FIG. 10. (Color online) Schematic representation of the singularities Ω_i/Z evolution between $\theta_k=0$ and $\pi/2$. Proper scale is not preserved.

$>\sqrt{3}\rho_{p\perp}$, the instability is Weibel-like and no longer needs the beam to develop so that transverse beam temperature no longer affects it.

B. Critical directions

The inventory of the singularities gathers the Ω_{1234} singularities of the isotropic plasma mentioned by Eqs. (44) together with the following singularities arising from the isotropic beam (singularities arising from the parallel beam temperature are simplified as in Sec. IV C):

$$\Omega_5 = Z\cos\theta_{\mathbf{k}} - Z\frac{\rho_{b\perp}}{\gamma_b}\sin\theta_{\mathbf{k}} - Z\frac{\rho_{b\parallel}}{\gamma_b^3}\cos\theta_{\mathbf{k}},$$

$$\Omega_6 = Z\cos\theta_{\mathbf{k}} - Z\frac{\rho_{b\perp}}{\gamma_b}\sin\theta_{\mathbf{k}} + Z\frac{\rho_{b\parallel}}{\gamma_b^3}\cos\theta_{\mathbf{k}},$$

$$\Omega_7 = Z\cos\theta_{\mathbf{k}} + Z\frac{\rho_{b\perp}}{\gamma_b}\sin\theta_{\mathbf{k}} - Z\frac{\rho_{b\parallel}}{\gamma_b^3}\cos\theta_{\mathbf{k}},$$

$$\Omega_8 = Z\cos\theta_{\mathbf{k}} + Z\frac{\rho_{b\perp}}{\gamma_b}\sin\theta_{\mathbf{k}} + Z\frac{\rho_{b\parallel}}{\gamma_b^3}\cos\theta_{\mathbf{k}}. \quad (49)$$

As far as the critical angles are concerned, Fig. 10 sketches the evolution of the singularities Ω_i from $\theta_k=0$ to $\pi/2$. For $\theta_k=0$, the root yielding the two-stream instability appears (marginal stability) with its real part below Ω_5. As the angle increases, the marginal stability point is "squeezed" between Ω_5 and Ω_4, and then between Ω_5 and Ω_3. We therefore recover two critical angles $\theta_{c1,2}$ corresponding to $\Omega_5=\Omega_4$ and $\Omega_5=\Omega_3$, respectively,

$$\theta_{c1,2} = \arctan\left(\frac{1+\alpha \mp \rho_{p\parallel} - \rho_{b\parallel}/\gamma_b^3}{\rho_{p\perp} + \rho_{b\perp}/\gamma_b}\right), \quad (50)$$

where the "−" stands for θ_{c1} and the "+" for θ_{c2}. One can notice in Eq. (50) how parallel and transverse temperature play a symmetric role as the former appears at the numerator of the expression while the latter appears at the denominator. Also, Fig. 10 makes it clear that parallel temperature defines the singularities for $\theta_k=0$, whereas transverse temperature defines them for $\theta_k=\pi/2$. Equation (50) therefore represents the most general expression of the critical angle(s), and one can check how Eqs. (13), (27), (37), and (45) stand as a particular case of this one. The physical interpretation of these critical angles is simple. Each one corresponds to some points of joined resonance between some electrons from the beam and some others from the plasma. The resonances by themselves occur when the coupling between some electrons and the unstable mode is maximal because these electrons travel at the same speed as the wave. The overlapping of two singularities means that modes realizing such coincidence are perfectly coupled to a given electron population from the beam and the other from the plasma.

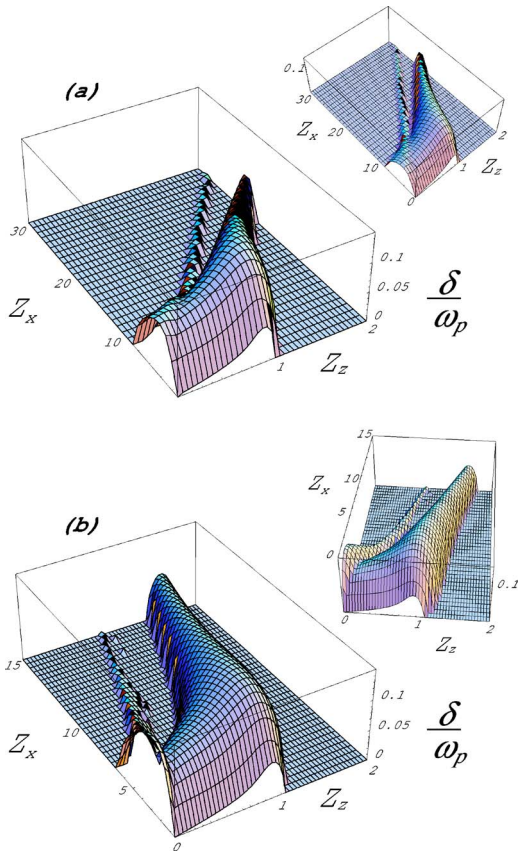

FIG. 11. (Color online) Evaluation of the growth rate all over the TSF branch for an isotropic plasma (a) with $\rho_{p\perp}=\rho_{p\parallel}=0.15$. (b) is plotted for an anisotropic plasma with $\rho_{p\perp}=0.05$ and $\rho_{p\parallel}=0.2$. Other parameters are $\alpha=0.05$, $\gamma_b=4$, and $\rho_{b\perp}=\rho_{b\parallel}=0.1$ for both plots. The figures are displayed from two points of view for a better appreciation of the filamentation/Weibel transition as well as the critical angles.

C. Arbitrary wave vector orientation

We first evaluated the growth rate for the "isotropic" case of an isotropically hot relativistic beam hitting an isotropically hot plasma and display the result in Fig. 11(a). Consid-

ering previous results, we expect the major temperature effect to be a reduction of the filamentation instability, and that is what is observed. With a plasma temperature $\rho_{p\perp}=\rho_{p\parallel}=0.15$ and a beam temperature $\rho_{b\perp}=\rho_{b\parallel}=0.1$, the absolute maximum growth rate is still 91% of the basic result obtained with a cold beam and a transversely hot plasma [see Eq. (12)]. Indeed, a fluid model uncovers the same maximum growth rate but does not recover *one* maximum [19]. It is therefore remarkable to observe that as far as the maximum growth rate is concerned, a simple fluid model yields a result which is quite close to a nonrelativistic temperature model.

We finally evaluate the growth rate in a situation very similar to the one corresponding to Fig. 8 and yielding a Weibel-like filamentation. We therefore chose almost the same plasma parameters with $\rho_{p\perp} \ll \rho_{p\parallel}$. The results, displayed in Fig. 11(b), show how beam temperature interferes with the plasma anisotropy. The instability domain beyond the critical angles is dramatically shrunk but the critical directions remain clearly visible. With a maximum growth rate still located "inside" the (Z_x, Z_z) plan (though filamentation/Weibel growth rate here is comparable), and still more than 90% of the basic expression given by Eq. (12), the most unstable mode located in the two-stream region eventually stands almost unaffected by temperature.

VII. CONCLUSION AND DISCUSSION

We have conducted a systematic investigation of temperature effects upon the unstable electromagnetic waves ranging from two-stream to filamentation modes. The first point we need to stress is that the maximum growth rate found with a quite basic model of reality, namely cold relativistic beam + transversely hot plasma, is robust enough to endure many temperature effects because of its two-stream-like properties. The maximum growth rate value can even be recovered through a cold plasma/beam (fluid) model, although its localization into *one* most unstable mode shall be lost. Surprisingly, parallel beam temperature does not affect the picture very much. This can be understood in terms of energy spread versus velocity spread. Since mode instability is a matter of wave-particle resonance, growth rates are very sensitive to the velocity spread. But for a relativistic beam, the parallel momentum spread yielding the parallel temperature eventually results in a small velocity spread so that waves tend to see a cold beam in the parallel direction.

If we now turn to the broader picture of the growth rate map all over the **k** space, temperature effects are numerous. To start with, parallel plasma temperature induces two critical angles instead of one. The two-stream region corresponds in this case to the modes located below the smallest angle. This region is eventually poorly affected by any temperature of any kind. On the other hand, the region beyond the smallest critical angle is mostly sensitive to beam transverse temperature and plasma parallel temperature. The first one has a strong stabilizing effect throughout this filamentation zone, whether it be in terms of the instability domain or in terms of the maximum growth rate. The second one can have a very interesting influence on the filamentation instability when plasma temperature anisotropy is strong. In this case, plasma parallel temperature induces a smooth transition from the beam based filamentation instability to the temperature anisotropy based Weibel instability. Both are purely transverse and have $\theta_k=\pi/2$, but filamentation growth rate is $\sim\beta\sqrt{\alpha/\gamma_b}$ (beam-dependent, no temperature dependence) while Weibel growth rate is here $\sim\beta\rho_{p\parallel}/\sqrt{3}$ (only plasma dependent). This shows that the three main instabilities of an unmagnetized plasma are eventually strongly connected to each other and are found here on the very same branch of the dispersion equation so that one can switch continuously from one to the other. As long as the filamentation/Weibel instability is "filamentation-like," it can be suppressed through transverse beam temperature. But when it becomes "Weibel-like," it disconnects from the beam and can no longer be suppressed by transverse beam temperature.

Finally, let us discuss the waterbag distribution approximation we are using here. It is intuitively obvious that it can model velocity dispersion, and it leads to analytically calculable quadratures more frequently than a Maxwellian. It is therefore often used to derive exact results, as Lorentzian can do it [26]. But how far exactly can one go with waterbag distributions? Let us define

$$W(x,T)=\frac{1}{2T}[\Theta(x+T)-\Theta(x-T)],$$

$$F(x,T)=\frac{1}{T\sqrt{\pi}}\exp(-x^2/T^2), \tag{51}$$

and compare the successive moments for both distributions,

$$\mathcal{M}_{W,n}(T)=\int_{-\infty}^{\infty}Wx^n dx=\frac{1+(-1)^n}{2}T^n\frac{1}{1+n},$$

$$\mathcal{M}_{F,n}(T)=\int_{-\infty}^{\infty}Fx^n dx=\frac{1+(-1)^n}{2}T^n\frac{\Gamma((1+n)/2)}{\sqrt{\pi}}, \tag{52}$$

where $\Gamma(x)$ is the Gamma function with $\Gamma(n)=(n-1)!$ [the moments are relevant because they may appear directly in the calculations of any $\int gW$ where the function g is expressed as $g(x)=\Sigma a_k x^k$]. We see here the odd moments are all equal (=0) whereas even moments depart from each other as $\mathcal{M}_F/\mathcal{M}_W$ diverges quite rapidly with n. Better performances can be achieved defining an equivalent waterbag temperature T_{Weq} such as when the second moments (mean kinetic energy) are equal. One needs therefore to consider $T_{Weq}=\sqrt{3/2}T$. Doing so, the ratio $\mathcal{M}_F/\mathcal{M}_W$ diverges less rapidly, but still does, and the three first moments are equal. Discrepancies between waterbags and Maxwellians tend therefore to happen for high moments, due to the infinite tail of the Maxwellian. Also, moment n being proportional to T^n, it is obvious that differences are all the more reduced when temperature is low. Indeed, both functions tend to $\delta(x)$ in the zero-temperature limit.

In the present case, we have to deal with the reduced temperatures defined by Eqs. (7) rather than with temperatures themselves. Let us consider the Maxwellian distribution

$$F = \frac{n_p}{\pi P_{tp\perp} P_{tp\parallel}} \exp\left[\frac{-p_x^2}{P_{tp\perp}^2} - \frac{(p_z + P_p)^2}{P_{tp\parallel}^2}\right] + \frac{n_b}{\pi P_{tb\perp} P_{tb\parallel}} \exp\left[\frac{-p_x^2}{P_{tb\perp}^2} - \frac{(p_z - P_b)^2}{P_{tb\parallel}^2}\right], \quad (53)$$

where we drop the p_y variable because it yields quadratures which can be calculated separately as long as temperatures are nonrelativistic. We then shall have to deal with a distribution function G in term of the reduced variables (7) such as

$$G \propto \frac{1}{\rho_{p\perp}\rho_{p\parallel}} \exp\left[\frac{-x^2}{(\rho_{p\perp}/\gamma_b)^2} - \frac{(z + \alpha/\gamma_b)^2}{(\rho_{p\parallel}/\gamma_b)^2}\right] + \frac{\alpha}{\rho_{b\perp}\rho_{b\parallel}} \exp\left[\frac{-x^2}{(\rho_{b\perp}/\gamma_b)^2} - \frac{(z-1)^2}{(\rho_{b\parallel}/\gamma_b)^2}\right], \quad (54)$$

where variables x and z are obtained from p_x and p_z through $p_x = xP_b$ and $p_z = zP_b$, the range of integration involved in every quadrature encountered remaining $(-\infty, \infty)$. It comes directly from this expression that the temperature parameters involved have the form ρ/γ_b. Therefore, these quantities are all the more small when the ρ's are nonrelativistic and $\gamma_b > 1$. This contributes greatly to the agreement between waterbags and Maxwellian results so that a good agreement is therefore to be expected, qualitatively and even quantitatively. As a matter of fact, it can be checked that Maxwellian low-temperature growth rates derived for two-stream and filamentation instabilities correspond to the ones obtained with waterbags, even for a nonrelativistic beam (see [6] for example). If we now turn to the Weibel instability, which is independent of the beam, the growth rate derived with waterbag distributions is the same as the growth rate derived with a Maxwellian in [2]. Only a factor $1/\sqrt{3}$ separates the two results, which can be improved to a factor $1/\sqrt{2}$ using the equivalent temperature T_{Weq} for the waterbag distribution.

One of the qualitative differences that can be expected has to do with the growth rate behavior in the critical angle. The unbounded character of the instability domain (at least for our base model) in this direction can be directly traced back to the existence of singularities in the Hilbert transform $\mathcal{H}(f) = (1/\pi) PP \int dt f(t)/(t-x)$ of the waterbag [17]. In the case of a Maxwellian, the Hilbert transform has no singularities. The instability domain in the critical directions should therefore be closed when Maxwellians are accounted for. One may ask whether or not there shall still be some critical angles in this case. The answer is yes because as long as temperatures are kept small, $\mathcal{H}(Mt^n)$ has maxima which roughly coincide with the singularities of $\mathcal{H}(Wt^n)$. We shall therefore recover some critical angles when two maxima overlap instead of two singularities, although the angle shall not be the same.

Another issue which could affect the growth rate behavior is the shape of the distributions defined by Eqs. (46). Such functions yield quadratures more easily calculable, but they define rectangles rather than ellipses in the momentum space so that some equal parallel and normal temperatures yield a square instead of an isotropic circle. The two kinds of distributions are sketched in Fig. 12, where the light gray squares

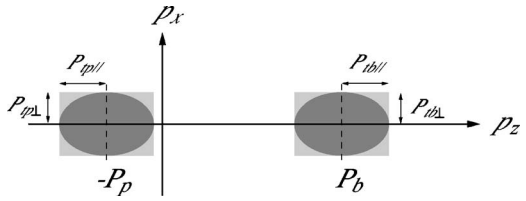

FIG. 12. Schematic representation of the distribution function in the momentum space. Functions defined by Eqs. (46) correspond to the light gray rectangle. When compared with isotropic distributions, strong gray ellipses, it can be considered that some electrons are added "in the corners."

stand for the functions used in this paper. One can therefore consider that we are adding some extra electrons "in the corners," from the rectangle up to the ellipsoid shape. How can these extra particles affect the present results? We can start noticing there are no extra particles at all to deal with when analyzing one temperature effect at a time. Results presented at the end of Sec. II as well as Secs. III and IV are insensitive to this feature. Also, Eq. (50) shows there are two critical angles even when considering only plasma parallel and beam normal temperatures, namely another case when rectangular and ellipsoidal distributions merge. Simply put, the critical angle(s) existing when the beam or the plasma are hot in only one direction cannot suddenly vanish as soon as temperature is added in another direction, regardless of the overall shape of the distribution. The existence of critical angles, as well as the localization of the maximum growth rate away from the main wave-vector axis, should therefore not be canceled when considering ellipsoidal waterbags instead of rectangular ones. Furthermore, the critical angle feature, or the very interesting filamentation/Weibel transition unraveled in Sec. V, both receive a clear physical interpretation showing the present analysis is describing real physical phenomena rather than some cuboidal waterbag artifacts.

Finally, let us review the last source of discrepancies between the use of Maxwellians and waterbags. It is somehow also related to the Hilbert transform problem and comes with the proper way of calculating the quadratures involved in Eq. (1) for the dielectric tensor. When calculating quadratures such as $\int dt f(t)/(t-x)$, we know since Landau that the physical way to give meaning to this integral consists in assuming first that we work with a collisional plasma. Adding a collisional term to the Vlasov equation, one needs therefore to evaluate quadratures such as $\int dt f(t)/(t-x-i\nu)$ with $\nu > 0$ [31]. The collisionless limit is then obtained through $\nu \to 0$ with

$$\lim_{\nu \to 0} \int_{-\infty}^{\infty} \frac{f(t)dt}{t - x - i\nu} = \pi \mathcal{H}(f) + i\pi f(x). \quad (55)$$

In a stable Maxwell plasma, the complex part of this result is precisely the one yielding the Landau damping. It turns out that this term vanishes exactly when using waterbag distributions so that Landau damping is impossible to model with these functions. But in an unstable plasma with small temperature, the dispersion equation is mainly driven by the real part of Eq. (55) because its imaginary part behaves as

$\exp(-1/T)$. This is why both filamentation and two-stream growth rates calculated with Maxwellians coincide with their waterbag counterpart for low temperatures.

It eventually appears that waterbag results can be trusted for low temperatures, which just means in the present setting nonrelativistic temperatures. This is not surprising since both distribution functions join at zero temperature. Although waterbags shall certainly give a good qualitative picture of things for relativistic temperatures, it seems that Maxwellians shall be needed there in order to retrieve correct quantitative, and maybe even qualitative, predictions.

ACKNOWLEDGMENTS

One of us (A.B.) wishes to thank the Laboratoire de Physique des Gaz et des Plasmas at Orsay University for allowing him to start this work. The work has been partially achieved under project FTN2003-00721 of the Spanish Ministerio de Educación y Ciencia.

APPENDIX: DISPERSION EQUATION FOR THE FILAMENTATION INSTABILITY

By setting $k_z=0$ in Eqs. (1) and (5), we get the following expression of the dispersion equation for the relativistic filamentation instability. The plasma is hot with $\rho_{p\perp}$ and $\rho_{p\parallel}$ transverse and parallel temperature. The dispersion equation with a beam hot in both directions is too large to be reported here, so that the equation below has the beam hot only in the transverse direction with temperature $\rho_{b\perp}$,

$$0 = -\alpha^2 Z_x^2 \left(\frac{\gamma_b}{Z_x^2\rho_{b\perp}^2 - \Omega^2\gamma_b^2} + \frac{1}{\Omega^2 - Z_x^2\rho_{p\perp}^2} \right)^2 + \left(1 + \frac{\alpha\gamma_b}{Z_x^2\rho_{b\perp}^2 - \Omega^2\gamma_b^2} - \frac{1}{\Omega^2 - Z_x^2\rho_{p\perp}^2} \right) \left[\Omega^2 - \frac{Z_x^2}{\beta^2} - \frac{\alpha}{\gamma_b^3} - \frac{\alpha\gamma_b Z_x^2}{\Omega^2\gamma_b^2 - Z_x^2\rho_{b\perp}^2} - \frac{x^2 + Z_x^2(\alpha^2 - \rho_{p\perp}^2 + \rho_{p\parallel}^2/3)}{\Omega^2 - Z_x^2\rho_{p\perp}^2} \right]. \quad \text{(A1)}$$

[1] M. Tabak, J. Hammer, M. E. Glinsky, W. L. Kruer, S. C. Wilks, J. Woodworth, E. M. Campbell, M. D. Perry, and R. J. Mason, Phys. Plasmas **1**, 1626 (1994).
[2] E. S. Weibel, Phys. Rev. Lett. **2**, 83 (1959).
[3] L. O. Silva, R. A. Fonseca, J. W. Tonge, W. B. Mori, and J. M. Dawson, Phys. Plasmas **9**, 2458 (2002).
[4] T. Okada and K. Niu, J. Plasma Phys. **24**, 483 (1980).
[5] A. Bret, M.-C. Firpo, and C. Deutsch, Phys. Rev. Lett. **94**, 115002 (2005).
[6] T. Okada and W. Schmidt, J. Plasma Phys. **37**, 373 (1987).
[7] M. Honda, Phys. Rev. E **69**, 016401 (2004).
[8] J. Fuchs, T. E. Cowan, P. Audebert, H. Ruhl, L. Gremillet, A. Kemp, M. Allen, A. Blazevic, J.-C. Gauthier, M. Geissel, M. Hegelich, S. Karsch, P. Parks, M. Roth, Y. Sentoku, R. Stephens, and E. M. Campbell, Phys. Rev. Lett. **91**, 255002 (2003).
[9] M. Tatarakis, F. N. Beg, E. L. Clark, A. E. Dangor, R. D. Edwards, R. G. Evans, T. J. Goldsack, K. W. D. Ledingham, P. A. Norreys, M. A. Sinclair, M-S. Wei, M. Zepf, and K. Krushelnick, Phys. Rev. Lett. **90**, 175001 (2003).
[10] Y. Sentoku, K. Mima, P. Kaw, and K. Nishikawa, Phys. Rev. Lett. **90**, 155001 (2003).
[11] R. A. Fonseca, L. O. Silva, J. W. Tonge, W. B. Mori, and J. M. Dawson, Phys. Plasmas **10**, 1979 (2003).
[12] E. S. Dodd, R. G. Hemker, C.-K. Huang, S. Wang, C. Ren, W. B. Mori, S. Lee, and T. Katsouleas, Phys. Rev. Lett. **88**, 125001 (2002).
[13] A. Pukhov and J. Meyer-ter-Vehn, Phys. Rev. Lett. **79**, 2686 (1997).
[14] M. Honda, J. Meyer-ter-Vehn, and A. Pukhov, Phys. Rev. Lett. **85**, 2128 (2000).
[15] H. Ruhl, A. Macchi, P. Mulser, F. Cornolti, and S. Hain, Phys. Rev. Lett. **82**, 2095 (1999).
[16] R. A. Fonseca, L. O. Silva, J. Tonge, R. G. Hemker, W. B. Mori, and J. M. Dawson, IEEE Trans. Plasma Sci. **30**, 1 (2002).
[17] A. Bret, M.-C. Firpo, and C. Deutsch, Phys. Rev. E **70**, 046401 (2004).
[18] B. B. Godfrey, W. R. Shanahan, and L. E. Thode, Phys. Fluids **18**, 346 (1975).
[19] F. Califano, R. Prandi, F. Pegoraro, and S. V. Bulanov, Phys. Rev. E **58**, 7837 (1998).
[20] S. Ichimaru, *Basic Principles of Plasma Physics* (W. A. Benjamin, Inc., Reading, MA, 1973).
[21] T. Okada, T. Yabe, and K. Niu, J. Phys. Soc. Jpn. **43**, 1042 (1977).
[22] P. H. Yoon and R. C. Davidson, Phys. Rev. A **35**, 2718 (1987).
[23] J. Dawson, Phys. Fluids **4**, 869 (1961).
[24] A. B. Mikhailovskii, *Theory of Plasma Instabilities*, Vol. 1 (Consultant Bureau, New York, 1974).
[25] S. Humphries, *Charged Particle Beams* (John Wiley and Sons, New York, 1990).
[26] T. M. O'Neil and J. H. Malmberg, Phys. Fluids **11**, 1754 (1968).
[27] L. D. Landau and E. M. Lifshitz, *Course of Theoretical Physics, Physical Kinetics* (Pergamon Press, New York, 1981), Vol. 10.
[28] The upper bound of the velocity interval thus defined must obviously be adjusted if it is found larger than c.
[29] The distributions we are using here are not exactly isotropic when both parallel and normal temperatures are accounted for. See Sec. VII and Fig. 12 for a discussion of this point.
[30] Let us remind the reader that "filamentation/Weibel" stands here for a mode which can switch continuously from the beam-dependent filamentation instability to the original Weibel instability only relying on the plasma anisotropy.
[31] One can also assume the perturbation applied to the Vlasov equation starts infinitely small from $t=-\infty$ through a factor $e^{-\nu t}$, before having $\nu\to 0$. Both approaches yield the same result [27].